Integrated Modeling Framework to Quantify the Coastal Protection Services Supplied by Vegetation

Greg Guannel, The Natural Capital Project, Stanford University, 371 Serra Mall, Stanford, CA 94305-5020 USA

Peter Ruggiero, College of Earth, Ocean, and Atmospheric Sciences, 104 CEOAS Administration Building, Oregon State University, Corvallis, OR 97331-5503

Joe Faries, The Natural Capital Project, Stanford University, Stanford University, 371 Serra Mall, Stanford, CA 94305-5020 USA

Katie Arkema, The Natural Capital Project, Stanford University, c/o School of Environmental and Forest Sciences, University of Washington, Box 352100, Seattle, WA 98195

Malin Pinsky, Department of Ecology, Evolution, and Natural Resources, and Institute of Marine and Coastal Sciences, Rutgers University, New Brunswick, NJ 08901-8551

Guy Gelfenbaum, U.S. Geological Survey Pacific Coastal and Marine Science Center, 400 Natural Bridges Drive, Santa Cruz, CA 95060

Anne Guerry, The Natural Capital Project, Stanford University, c/o School of Environmental and Forest Sciences, University of Washington, Box 352100, Seattle, WA 98195

Choong-Ki Kim, Maritime Safety Research Division, Korea Research Institute of Ships & Ocean Engineering, 1312-32, Yuseong-daero, Yuseong-gu, Daejeon 305-343 SOUTH-KOREA

Corresponding Author: G. Guannel, The Natural Capital Project, Stanford University, 371 Serra

Mall, Stanford, CA 94305-5020 USA (gguannel@stanford.edu)

Key Points:

- A novel approach models processes that measure vegetation protective services

- Vegetation has the potential to reduce water levels and erosion during storms

- Drag coefficient uncertainty yields large variability in protection estimates

Abstract: Vegetation can protect communities by reducing nearshore wave height and altering

sediment transport processes. However, quantitative approaches for evaluating the coastal

protection services, or benefits, supplied by vegetation to people in a wide range of coastal

environments are lacking. To begin to fill this knowledge gap, an integrated modeling approach

is proposed for quantifying how vegetation modifies nearshore processes – including the

attenuation of wave height, mean and total water level – and reduces shoreline erosion during

storms. We apply the model to idealized seagrass-sand and mangrove-mud cases, illustrating its

potential by quantifying how those habitats reduce water levels and sediment loss beyond what

would be observed in the absence of vegetation. The integrated modeling approach provides an

efficient way to quantify the coastal protection services supplied by vegetation and highlights

specific research needs for improved representations of the ways in which vegetation modifies

wave-induced processes.

Index Terms and Keywords: coastal processes, sediment transport, uncertainty, wetlands, coastal vegetation, wave setup and runup, coastal erosion, mud bed scour, coastal protection ecosystem services

1   Introduction

Coastal vegetation (e.g., seagrass beds, kelp forests, marshes, mangroves and coastal forests) protects shorelines, human development, and economic activity by reducing the impacts of coastal hazards. Specifically, vegetation has been shown to attenuate wave height, moderate the strength of wave-induced currents and decrease the extent of wave runup on beaches [*Lovas and Torum*, 2001; *Bridges*, 2008; *Luhar et al.*, 2010]. These effects result in lower water levels and reduced shoreline erosion, functional benefits that can save lives, and prevent millions of dollars in property damage [*Mazda et al.*, 1997; *Das and Vincent*, 2009].

The most commonly reported measure of the coastal protection services, or benefits, provided by vegetation to people is the attenuation of wave height. The use of that metric has been facilitated by the wide availability of engineering models for wave evolution in the presence of vegetation (see, e.g., *Suzuki et al.*[2012], or reviews from *Anderson et al.* [2011] and *McIvor et al.* [2012]). However, some of the most important coastal protection metrics needed by engineers and scientists are the amount of avoided coastal erosion and inundation during storms due to the presence of vegetation. To compute these metrics, it is necessary to quantify how different plants, under storm forcing conditions, alter total water levels and the erosion processes of sandy or muddy shorelines.

Most of the numerical models that examine the detailed response and impacts of particular types of vegetation on nearshore processes and on the shoreline are often developed for specific habitats under specific settings (see, e.g., *Augustin et al.* [2009], *Li and Zhang*

[2010], or *Maza et al.* [2013]). Even when general approaches are proposed to quantify how vegetation alters sediment transport and shoreline erosion, they consider only a limited range of vegetation types, rely heavily on models suited for sandy beaches devoid of vegetation, or are too complex for general use [*Chen et al.*, 2007; *Mariotti and Fagherazzi*, 2010; *Karambas et al.*, 2012]. Some of these deficiencies are attributable to an incomplete understanding of the way in which vegetation modifies sediment transport processes [*Le Hir et al.*, 2007]. However, these deficiencies are also due to the absence of a modeling framework that links all the relevant processes governing the interaction of waves and vegetation.

In a first step toward filling this gap, we introduce an integrated modeling framework to quantify how vegetation attenuates wave energy, moderates water levels, and avoids sand or mud loss during storms. This modeling approach relies on well-established models and modifications thereof, links the most relevant processes responsible for inundation and shoreline erosion, and provides an initial practical framework for deepening our understanding of how vegetation alters key nearshore processes and thus supplies coastal protection services to people. Ultimately, the service of coastal protection is supplied by the biophysical processes modeled here in addition to the social and economic factors (e.g., where people live and the value of coastal property) that influence where and how people actually benefit from the avoided loss of sand or mud during storms [*Tallis et al.*, 2012].

This paper is organized into four sections. Section 2 presents the details of the proposed framework. Section 3 presents the results of the application of the model to two idealized cases: a sandy shoreline with a nearshore seagrass meadow and a mangrove forest growing on a mud bed. Throughout, we highlight where more research is needed to reduce the uncertainty in our estimates. Section 4 presents the conclusion.

2   Nearshore Wave and Erosion Model

Vegetation supplies coastal protection services by modifying nearshore waves, water levels and sediment transport. In this section, we present the framework of a process-based model to quantify these services. After defining the study domain and the model's main variables, we briefly review the computational method for the evolution of a wave field in the presence of vegetation. Then we describe methods to estimate mean and total water levels at the shoreline as well as the amount of beach retreat or mud bed scour in the presence of vegetation. Throughout, we highlight our assumptions, the model's limitations, and, importantly, key areas for future improvements.

2.1   Model Setup and Definition of Variables

The study domain is defined in a longshore uniform, two-dimensional vertical (2DV) coordinate system (x, z), with x pointing shoreward, z pointing upwards and the origin at the still water level (Figure 1; see also Table 1 for a list of commonly used symbols). The coast may either be sandy or muddy. Wave properties, such as the free surface elevation η, are expressed using linear wave theory (LWT). Wave crests are propagating parallel to the coast and are modeled along a shore-perpendicular one-dimensional transect. Two-dimensional processes, including longshore currents, are assumed negligible.

A storm approaching the region of interest generates a wave field with a deep-water significant wave height H_o, peak period T_p, and horizontal and vertical water particles velocities u and w, respectively. Velocity component are decomposed into short-wave and mean values [*Svendsen*, 2006], ignoring turbulent motions, e.g., $u = u_{ow} \cos \psi + U$, where u_{ow} is the short-wave amplitude, $\psi(x, t)$ the wave phase and t represents time. U is the time averaged velocity,

$U = \bar{u}$, and it is weak compared to the short-wave velocity: $|U|/u_{ow} < 1$ and $(U/u_{ow})^2 \ll 1$

[*Svendsen*, 2006]. Finally, the near bed mean velocity is expressed as U_b.

As waves progress shoreward, they encounter a vegetation field (e.g., a seagrass meadow, marsh, or a mangrove forest). Marshes and seagrass meadows have single stems, with diameter d_v, height h_v and a density of N_v stems per m^2 (Figure 1). Mangroves and forests may have supra-aerial roots, trunk and canopies. Each of these components has a diameter d_{vi}, height h_{vi} and density N_{vi}, where the subscript *i* represents roots, trunk or canopy.

Vegetation stems do not sway with the flow, and are represented by vertical cylinders of uniform diameter [*Dalrymple et al.*, 1984]. Thus waves exert a horizontal drag force F_d on the stems in the cross-shore direction [*Dalrymple et al.*, 1984]:

$$\overrightarrow{F_d} = \frac{1}{2}\rho C_d d_v N_v \vec{u}|\vec{u}| \tag{1}$$

where C_d is a drag coefficient associated with the vegetation field. Estimates of the drag force F_d using LWT in Equation (1) can differ substantially from more accurate computational approaches (Appendix A).

Storms often generate surges at the shoreline, which can be altered by vegetation. However, since the primary focus of this paper is the modification of wave processes by vegetation, we neglect surge attenuation by plants and refer interested readers to, e.g., *Wamsley et al.* [2010] or *Zhang et al.* [2012].

2.2   Wave model

The evolution of a wave field of root-mean square (rms) wave height H in a 2DV coordinate system with weak mean currents is computed by solving the wave energy balance equation:

$$\frac{\partial E_w C_g}{\partial x} = -D_b - D_f - D_v \tag{2}$$

where E_w is the wave energy density and C_g the group velocity. The dissipation of wave energy flux is caused by wave breaking (D_b), bottom friction (D_f), and the presence of vegetation in the water column (D_v). D_b and D_f are expressed following *Thornton and Guza* [1983]:

$$D_b = \frac{3}{32\sqrt{\pi}} \rho g \frac{\sigma b^3}{\gamma h^5} H^7 \tag{3}$$

$$D_f = \frac{C_f}{16\sqrt{\pi}} \left(\frac{\sigma}{\sinh kh} \right)^3 H^3 \tag{4}$$

where ρ is the water density, g the constant of gravity, k the wavenumber and σ the wave frequency. The breaking coefficient b and breaker index γ have default values of 1.0 [*Thornton and Guza*, 1983] and 0.78 [*Dean and Dalrymple*, 1984], respectively.

D_f is the transfer of wave energy flux to the turbulent bottom boundary layer, in the

absence of vegetation, and C_f is a bottom friction coefficient, typically a function of bed

roughness. Because D_f is usually small, we ignore the presence of vegetation in Equation (4)

(see, e.g., *Nepf* [1999]), and use a default value of $C_f = 0.01$ for sand beds [*Thornton and Guza*,

1983]. For mud beds, $C_f = 2.08\text{x}10^{-3}\left(u_b^2/\sigma\right)^{-0.187}$ [*Whitehouse et al.*, 2001]. (We performed a

sensitivity analysis (not shown) to the expression of C_f, following recommendations in, e.g.,

Nielsen [1992] and *Whitehouse et al.* [2001], and found that the expression of that coefficient

had little impact on the final results since dissipation of wave energy via bottom friction is small

in comparison to the other dissipative mechanisms.)

Finally, dissipation due to vegetation D_v is expressed as [*Suzuki et al.*, 2012]:

$$D_v = \frac{1}{2\sqrt{\pi}}\rho\left(\frac{kg}{2\sigma}\right)^3\frac{\sum_{i=1}^{3}D_{vi}}{3k\cosh^3 kh}H^3 \qquad (5)$$

where, for mangroves and trees, $D_{vi,i=1-3}$ represent the contributions of roots ($i = 1$), trunk ($i = 2$)

and canopy ($i = 3$). Detailed expressions for $D_{vi,i=1-3}$ are provided in Appendix B. For seagrasses

and marshes, $i \equiv 1$ to represent stems, and the expression of D_v is identical to the expression of

Mendez and Losada [2004].

Equation (5) has been extensively validated (see, e.g., *Pinsky et al.* [2013]). It assumes

that dissipation is dominated by short-wave forces and neglects the role of mean currents, wave

reflection and other non-linear processes that occur near and within vegetated fields. Outputs from Equation (2) are used to estimate the total water level at the shoreline.

2.3   Total Water Level Model

The total water level at the shoreline is a critical driver of coastal flooding and shoreline erosion. It is, in part, a function of the astronomical tide, the storm surge, and the runup level of waves [*Ruggiero et al.*, 2001]. The runup is the sum of the wave setup at the shoreline and the height of the incident and infragravity band swash [*Stockdon et al.*, 2006]. In this section, we first derive an equation for the mean water level in the presence of vegetation. Then we propose a method to compute wave runup on beaches in the presence of vegetation.

2.3.1   Computation of Wave Setup

Dean and Bender [2006] heuristically developed an expression for the mean water level $\bar{\eta}$ in the presence of vegetation by arguing that stems exert a stress on the water column, and by inserting that stress directly into the mean momentum equation. Here, we confirm that vegetation has the potential to modify $\bar{\eta}$ by deriving an expression for the mean momentum equation in the presence of vegetation, starting from the governing equations of fluid motion. We present this derivation for single stem vegetation elements in a monochromatic wave field, and then expand it to all vegetation types in a random wave field. Throughout, we highlight both theoretical and observational knowledge limitations and gaps that are necessary to fully validate and eventually improve that expression.

To express $\bar{\eta}$ in the presence of vegetation, it is necessary to first assume that the drag coefficients C_d in the momentum equation, Equation (7), and in the wave evolution equation, Equation (5), are identical. Similarly, C_d associated with short wave and mean velocities, u_{ow} and U, are identical [*Zhou and Graham*, 2000; *Luhar et al.*, 2010].

The 2DV conservation of mass and momentum equations in the presence of vegetation are [*Augustin et al.*, 2009; *Li and Zhang*, 2010]:

$$\frac{\partial u}{\partial x} + \frac{\partial w}{\partial z} = 0 \qquad (6)$$

$$\begin{cases} \rho\dfrac{\partial u}{\partial t} + \rho\dfrac{\partial u^2}{\partial x} + \rho\dfrac{\partial uw}{\partial z} = -\dfrac{\partial p}{\partial x} + \left(\dfrac{\partial \tau_{xx}}{\partial x} + \dfrac{\partial \tau_{zx}}{\partial z}\right) - F_d \\[2mm] \rho\dfrac{\partial w}{\partial t} + \rho\dfrac{\partial uw}{\partial x} + \rho\dfrac{\partial w^2}{\partial z} = -\dfrac{\partial p}{\partial z} - \rho g + \left(\dfrac{\partial \tau_{xz}}{\partial x} + \dfrac{\partial \tau_{zz}}{\partial z}\right) \end{cases} \qquad (7)$$

where p represents the hydrostatic pressure, and τ_{ij} represent the shear stress components, in tensor notation. The drag force F_d [Equation (7)] is only included in the horizontal component of the momentum equation. That force is null in the vertical direction since stems are treated as rigid vertical cylinders [*Dalrymple et al.*, 1984].

Equations (6) and (7) are integrated through the water column and time averaged, velocity is decomposed into oscillatory and mean components, and dynamic and kinematic boundary conditions are applied. For brevity, only calculations involving vegetation variables are shown below – interested readers are referred to *Longuet-Higgins and Stewart* [1963, 1964] or *Svendsen* [2006] for more details. These equations become, for steady state conditions:

$$\frac{\partial \bar{Q}}{\partial x} = 0 \tag{8}$$

$$\rho g \left(h + \bar{\eta}\right)\frac{\partial \bar{\eta}}{\partial x} + \frac{\partial S_{xx}}{\partial x} + \overline{\int_{-h}^{\eta} F_d \ \mathrm{d}z} + \tau_b = 0 \tag{9}$$

where Q is the shoreward mass flux of the waves, τ_b is the bottom shear stress, and S_{xx} is the

radiation stress generated by both waves and rollers. The energy of the roller E_r is modeled

following *Reniers and Battjes* [1997] and *Apotsos et al.* [2007].

Equation (8) indicates that, since $\bar{Q} \equiv 0$ at the coast, waves generate a steady current

$U(x,z)$, the undertow, with a depth averaged value $U_{Off}(x)$ that balances the shoreward mass

flux of waves [*Guannel and Özkan-Haller*, 2014]:

$$\rho h U_{Off} = -\frac{E_w + 2E_r}{C} \tag{10}$$

where C is the wave celerity. This equation indicates that, because vegetation reduces the

energy density of waves [Equation (2)], vegetation also moderates the depth-average undertow

U_{Off}. As the undertow is one of the principal mechanisms for offshore sediment transport during

storms [*Guannel*, 2009], Equation (10) suggests that submerged vegetation is likely to reduce

coastal erosion.

The mean momentum equation, Equation (9), is identical to the classic expression

derived by *Longuet-Higgins and Stewart* [1963, 1964], with the addition of a stress term due to

the presence of vegetation elements $\widetilde{F_d} = \overline{\int_{-h}^{\eta} F_d \, dz}$. We express this variable by decomposing

$u|u|$ following *Svendsen* [2006, Ch. 10]:

$$\widetilde{F_d} = \overline{\int_{-h}^{\eta} \frac{1}{2} \rho C_d d_v N_v u |u| dz} = \overline{\int_{-h}^{\eta} \Phi u |u| dz} = \overline{\int_{-h}^{\eta} \Phi \left(U u_{ow} \beta_1 + u_{ow}^2 \beta_2 \right) dz} \qquad (11)$$

where $\Phi = 1/2 \rho C_d d_v N_v$. Assuming that mean currents are weak (see Section 2.1),

$\beta_1(t) \cong |\cos \psi| \left[1 + U / (u_{ow} \cos \psi) \right]$ and $\beta_2(t) = \beta_1(t) \cos \psi$. After further algebraic

manipulations, $\widetilde{F_d}$ simplifies to:

$$\widetilde{F_d} \cong \Phi \overline{\int_{-h}^{\eta} u_{ow}^2 |\cos \psi| \cos \psi \, dz + \int_{-h}^{0} 2 U u_{ow} |\cos \psi| dz} \qquad (12)$$

where we used $(U / u_{ow})^2 \ll 1$ and confined the undertow between the still water level and the

bed [*Svendsen*, 2006; *Guannel and Özkan-Haller*, 2014].

Up to this point, Equation (12) can be solved using any wave theory. In the remainder of

this derivation, wave properties are represented using LWT in order to be consistent with the

derivation of Equation (2). It is important to note that, regardless of vegetation type, the use of

LWT can sometimes over- or under-estimate the exact value of the drag force [Equation (1)], of

the vegetation-induced stress [Equation (12)], and of the dissipation of wave energy due to the presence of vegetation [Equation (5)] (see Appendix A). These limitations are not restricted to the model presented herein, but to any LWT-based model –the question of model uncertainty is examined and discussed further in Section 3.

Using LWT, the first terms on the RHS of Equation (12) vanishes for submerged stems; it is non-zero if it is computed with a non-linear wave model [*Dean and Bender*, 2006]. However, as *Dean and Bender* [2006] have shown, vegetation reduces mean water level (see also Section 3). Consequently, in order to keep this important process into account, and to remain consistent in the use of LWT, we hereafter scale the short-wave stress generated by a submerged vegetation field by the stress generated by an identical emerged field:

$$\widetilde{F}_{d\ waves}^{veg,submerged} = \alpha_v \widetilde{F}_{d\ waves}^{veg,emerged} = \alpha_v \Phi \overline{\int_0^\eta u_{ow}^2 |\cos\psi| \cos\psi\, dz} \tag{13}$$

where $\alpha_v = \min\left(h_v / h, 1\right)$. This approximation is reasonable because $\alpha_v F_d$ values computed using LWT versus F_d values computed at various water depths using the more exact non-linear stream function theory [*Dean*, 1965] can be linearly related throughout the water column and at the water surface ($R^2 > 0.8$ and $R^2 > 0.9$, respectively; see Appendix A).

Assuming that the short-wave velocity is constant between the still-water level and the wave crest [*Dean and Bender*, 2006; *Svendsen*, 2006], Equation (12) becomes, for monochromatic waves:

$$\widetilde{F_d} \cong \Phi\left[\overline{\alpha_v u_{ow}^2 \eta \cos\psi |\cos\psi|} \quad + \int_{-h}^{\overline{-h(1-\alpha_v)}} 2Uu_{ow}|\cos\psi|\, dz \right]$$

$$\cong \Phi\left(\frac{\alpha_v gk}{6\pi \tanh kh} H_{mn}^3 + \frac{2U_{Veg}C\sinh(k\alpha_v h)}{\pi \sinh kh} H_{mn} \right) \qquad (14)$$

where H_{mn} is a monochromatic wave height representative of the wave field. In Equation (14),

the mean horizontal current within the vegetated field U_{Veg} is assumed, as a first approximation,

to be constant in the vertical [*Luhar et al.*, 2010]. This assumption is reasonable, based on

numerical simulations and observations [*Lovas and Torum*, 2001; *Maza et al.*, 2013]. It also

avoids including more complexity in the model, an approach justified by our limited

understanding of how vegetation modifies the undertow, as discussed in Section 3.

Substituting Equation (14) into Equation (9) yields:

$$\underbrace{\rho g(h+\bar{\eta})\frac{\partial \bar{\eta}}{\partial x} + \frac{\partial S_{xx}}{\partial x}}_{I} + \underbrace{\frac{1}{2}\rho C_d d_v N_v \frac{\alpha_v gk}{6\pi \tanh kh} H_{mn}^3}_{II} + \underbrace{\rho C_d d_v N_v \frac{U_{Veg}C\sinh(k\alpha_v h)}{\pi \sinh kh} H_{mn}}_{III} + \underbrace{\tau_b}_{IV} = \qquad (15)$$

The first term on the LHS [term *I*] represents the classic mean momentum balance in nearshore

regions without vegetation [*Dean and Dalrymple*, 1984]. Vegetation alters the mean water level

via the addition of a short-wave induced stress on the water column (term *II*), the advection of

mean currents (term *III*) and by changing the strength of the bed shear stress (term *IV*). Indeed,

the bed shear stress can be expressed as $\tau_b \cong 2/\pi\rho C_f u_{ow} U_b$ [*Svendsen*, 2006], which is likely

affected by the presence of vegetation (Equation (10), see also observations by, e.g., *Lovas and Torum* [2001] or *Luhar et al.* [2010]).

To generalize the expression for $\bar{\eta}$ to all vegetation types, the stresses associated with each layer that makes up the vegetated field (e.g., roots, trunk, canopies) are linearly added, following *Suzuki et al.* [2012] and the resulting equation is converted to random wave fields, following *Mendez and Losada* [2004]. We obtain:

$$\rho g\left(h+\bar{\eta}\right)\frac{\partial\bar{\eta}}{\partial x}+\frac{\partial S_{xx}}{\partial x}+\left(\frac{1}{16\sqrt{\pi}}\frac{\sum_{i=1}^{3}\rho C_{di}d_{vi}N_{vi}\alpha_{vi}gk}{\tanh kh}H^3+\frac{\sum_{i=1}^{3}\rho C_{di}d_{vi}N_{vi}U_{veg}CS_{vi}}{2\sqrt{\pi}\sinh kh}H\right)+\tau_b=0 \qquad (16)$$

where H is the rms wave height, and the subscript "i" represents roots, trunk or canopy. Expressions for the coefficients α_{vi} and S_{vi} are provided in Appendix B.

Finally, to remain consistent with the approximations used in the derivation of Equation (5), the mean current term is neglected (see, e.g., *Dalrymple et al.* [1984] and *Mendez and Losada* [2004]; see also Section 3 where the relative importance of the neglected mean current term is examined) to obtain:

$$\rho g\left(h+\bar{\eta}\right)\frac{\partial\bar{\eta}}{\partial x}+\frac{\partial S_{xx}}{\partial x}+\frac{1}{16\sqrt{\pi}}\frac{\sum_{i=1}^{3}\rho C_{di}d_{vi}N_{vi}\alpha_{vi}gk}{\tanh kh}H^3+\tau_b=0 \qquad (17)$$

For seagrasses and marshes, this equation becomes

$$\rho g \left(h + \bar{\eta}\right) \frac{\partial \bar{\eta}}{\partial x} + \frac{\partial S_{xx}}{\partial x} + \frac{1}{16\sqrt{\pi}} \rho C_d \frac{\alpha_v d_v N_v g k}{\tanh kh} H^3 + \tau_b = 0 \qquad (18)$$

Ignoring the bed shear stress and the presence of a roller, Equation (18) reduces to Equation (1) of *Dean and Bender* [2006], for monochromatic wave fields.

Equations (17) and (18) provide an approach for estimating the setup nearshore $\bar{\eta}_{shore}$ [$\bar{\eta}_{shore} = \bar{\eta}(x \approx shore)$], a significant component of the runup and total water level, in the presence of most vegetation types. While commonly used approximations were used to derive Equations (17), we are not aware of a dataset presently available to validate it. Outputs of this equation are used to estimate runup and total water level at the shoreline.

2.3.2   Wave Runup on Beaches

The 2% exceedence level of wave runup maxima generated by random wave fields on open coast sandy beaches in the absence of vegetation can be estimated by the expression proposed by *Stockdon et al.* [2006]:

$$R_u = 1.1 \left(0.35m\sqrt{H_o L_o} + \frac{\sqrt{0.563m^2 H_o L_o + 0.004 H_o L_o}}{2} \right) = 1.1 \left(\bar{\eta}_{St} + \frac{\sqrt{s_{inc}^2 + s_{ig}^2}}{2} \right) \qquad (19)$$

where L_o is the offshore wave length, and m the foreshore slope of the beach. This equation

expresses runup as a function of empirical estimates of incident wave setup at the shoreline $\overline{\eta}_{St}$,

and incident and infragravity band swash s_{inc} and s_{ig}. As shown by *Raubenheimer et al.* [2001],

this empirical estimate of setup is a priori different from the nearshore setup, $\overline{\eta}_{shore}$, computed

using the process-based model described by Equation (17).

We modify the empirical expression of runup to take into account the presence of

vegetation by first assuming that plants only affect setup and incident band swash; vegetation has

a limited impact on the propagation of infragravity waves (see observations in, e.g., *Möller et al.*

[1999], *Manca et al.* [2012], or *Jadhav et al.* [2013]), and thus on low frequency swash. Next, we

relate mean water level values nearshore computed in the presence and absence of vegetation

from Equation (17) by a proportionality coefficient ε : $\overline{\eta}_{shore}^{veg} = \varepsilon \overline{\eta}_{shore}$, where the superscript *veg*

indicates that vegetation is present. Then, we modify the empirical estimate of setup $\overline{\eta}_{St}$ at the

shoreline in Equation (19) to take into account the presence of vegetation by using the same

proportionality coefficient ε : $\overline{\eta}_{St}^{veg} = \varepsilon \overline{\eta}_{St}$. This approximation is justified by the fact that, in the

absence of vegetation, the nearshore setup $\overline{\eta}_{shore}$ can be linearly related to the empirical estimate

of setup $\overline{\eta}_{St}$ at the shoreline ($R^2 > 0.7$; Appendix C). Applying the same proportionality

coefficient ε to the incident swash variable, Equation (19) becomes, in the presence of

vegetation:

$$R_u = 1.1 \left(0.35 m \varepsilon \sqrt{H_o L_o} + \frac{\sqrt{0.563 m^2 \varepsilon^2 H_o L_o + 0.004 H_o L_o}}{2} \right) = 1.1 \left(\varepsilon \overline{\eta}_{St} + \frac{\sqrt{\varepsilon^2 s_{inc}^2 + s_{ig}^2}}{2} \right) \quad (20)$$

In cases where vegetation produces a setdown near the shoreline, $\varepsilon \equiv 0$, which is likely to under-estimate the potential for vegetation to reduce runup. While we justify the assumptions used herein in Appendix C, we are not aware of a dataset to validate Equation (20).

For sandy beaches, the runup is added to the storm surge to yield the total water level in the presence of vegetation. For mud beds, or in cases when dunes fail, swash processes are ignored and Equation (17) is used instead. Wave characteristics, mean and total water level values are used to compute shoreline change.

2.4   Coastal Change Model

The supply of coastal protection services by plants can be quantified by taking the difference in shoreline erosion observed in their presence and absence. In this section, we modify existing models developed in the absence of vegetation to estimate the amount of sandy beach retreat and mud bed scour in the presence of vegetation.

2.4.1   Erosion of Sandy Beaches

We compute the amount of beach erosion E_{beach} [m] during a storm in the presence of vegetation by adapting the erosion model of *Kriebel and Dean* [1993]:

$$E_{beach} = \Theta \frac{S_T \left(\tilde{x}_b - h_b / m \right) - W \left(B + h_b - S_T / 2 \right)}{B + D + h_b - S_T / 2} \quad (21)$$

where B and W are the beach berm height and width and D is the dune height (Figure 1). S_T is the total water level [*Mull and Ruggiero*, 2014], and h_b and $\tilde{x}_b$ represent the depth and distance from the shoreline of the breakpoint, respectively. Θ is a convolution integral that limits the beach erosional response as a function of wave breaking characteristics, storm duration, and a characteristic erosion time scale [*Kriebel and Dean*, 1993]. The location of wave breaking x_b is identified from the profile of wave height [Equation (2)] as $H(x_b) = \gamma h$. Consequently, changes in total water level and in breaking characteristics of incoming waves caused by vegetation dictate the amount of erosion modeled.

2.4.2   Erosion of Muddy Shores

Muddy shoreline erosion is a function of mud composition, plant biomass and physical characteristics, and of incident wave characteristics [*Whitehouse et al.*, 2001; *Feagin et al.*, 2009; *Mariotti and Fagherazzi*, 2010]. Here, we quantify the rate of mud bed scour E_{mud} [cm/hr] in the presence of vegetation by adapting the method presented in *Whitehouse et al.* [2001]:

$$E_{mud} = \begin{cases} 36(\tau - K_{veg}\tau_c)m_e C_m, & \tau > K_{veg}\tau_c \\ 0 & , & \tau \leq K_{veg}\tau_c \end{cases} \tag{22}$$

where m_e is the bed erosion constant, and C_m is the bed dry density, with typical values of 10^{-3} m.s^{-1} and 70 kg.m^{-3}, respectively [*Whitehouse et al.*, 2001; *Myrhaug et al.*, 2006]. The bed

shear stress is $\tau = \rho C_f u_{bed}^2$, where u_{bed} is the near-bed wave-induced velocity and C_f is a mud

friction factor (Section 2.2). The critical mud bed shear stress is $\tau_c = 5.42\mathrm{x}10^{-6} C_m^{2.28}$ [*Whitehouse*

et al., 2001]. Finally, plant biomass increases the critical shear stress of the mud by a factor

$K_{veg} = 4$ (no unit), following *Le Hir et al.* [2007] and *Mariotti and Fagherazzi* [2010].

In summary, we have proposed a modeling approach to quantify the supply of coastal

protection services by aquatic vegetation. In this approach, vegetation modifies the cross-shore

profile of wave height by dissipating wave energy [Equations (2) and (5)] and moderates the

total water level at the shoreline [Equations (17) and (20)]. Changes in wave height, mean and

total water level are translated into estimates of shoreline retreat and mud bed scour [Equations

(21) and (22)]. This integrated modeling framework is based on new derivations and

modifications of a mixture of theoretical and empirical formulations of nearshore hydrodynamics

in the presence and/or absence of vegetation. In the next section, this model is applied to two

simple illustrative examples.

3   Model Application

In this section, we first apply and test the robustness of the modeling framework by

quantifying the protective service of a seagrass meadow offshore of a sheltered sandy beach, and

of a mangrove forest on a mud bed, for 3 hypothetical storms (Table 2). For both vegetation

cases, wave properties (H, $\overline{\eta}_{shore}$, etc.) are computed from the offshore extent of the profile to

the nearshore, where the minimum water depth is 10 cm. Throughout, plant characteristics and

drag coefficient value, based on U.S. Federal Emergency Management Agency guidelines

(*FEMA* [2007]; see *Pinsky et al.* [2013] and Appendix D for other examples of formulations), are

kept constant. Next, we assess the sensitivity of the model to the uncertainty associated with the

choice of plant parameters and discuss the practical ramifications of the results.

3.1   Seagrass Meadow Fronting a Dune-backed Sandy Beach

In this example, a seagrass meadow grows from -5.0 to -0.5 m on a beach exhibiting an equilibrium profile. The beach has a 3 m high dune, a profile scale factor $A = 0.0115$, corresponding to a sand diameter $d_{50} = 0.25$ mm [*Dean and Dalrymple*, 2002, chap.7], and a 1V:15H foreshore slope (Figure 2d). The physical parameters of the seagrass are similar to the ones observed by *Huber* [2003], with $h_v = 40$ cm, $d_v = 0.6$ cm, and $N_v = 1,200$ stems/m^2 (Figure 1). In accordance with *FEMA* [2007], $C_d = 0.1$, which implicitly accounts for the plant flexibility.

3.1.1   Quantification of Coastal Protection Services

In this section, we first present detailed outputs for storm B (Table 2), which generates a surge of $S = 1.0$ m and a wave field with significant wave height $H_o = 2.5$ m and peak period $T = 6.0$ s. Next, we present results for the two other storms. Throughout, we compare model outputs obtained in the presence of vegetation to outputs obtained in the absence of vegetation.

During storm B, wave height is reduced over the vegetated field, relative to the situation with no vegetation present, by an average of 12%. The breaking wave height is reduced by 50% (Figure 2a). Analysis of the profile of wave height and breaking dissipation profiles (not shown) reveal that vegetation inhibits wave shoaling and decreases the amount of breaking dissipation in the surf zone. Consequently, the breaking wave height is reduced and the breakpoint is shifted closer to shore (Figure 2a), compared to the no-vegetation case. Three meters shoreward of the vegetation field, wave heights computed with and without vegetation are equal: the far field effects of the vegetation on wave height can be limited and local wave attenuation, in and of itself, is not a complete descriptor of the service provided by vegetation.

In addition to dissipating wave energy flux, the stems also reduce $\bar{\eta}$ throughout the surf zone, yielding a 41 cm, or 83%, reduction in setup nearshore ($\bar{\eta}_{shore}$, Figure 2b). If vegetation-induced stresses in the cross-shore momentum balance are ignored, $\bar{\eta}_{shore}$ still decreases by 12 cm, relative to the no-vegetation case, due to the influence of vegetation on the radiation stress gradient alone. Hence, regardless of the limitations of Equation (17), vegetation moderates the wave-induced mean water level, and hence the total water level. Note that we report values of $\bar{\eta}_{shore}$, the setup near the shoreline computed from Equation (18). This setup is modified to compute values of runup, and setup $\bar{\eta}_{St}$, from Equation (20) (see Section 2.3.2). In this example, values of $\bar{\eta}_{St}$ are lower than values of $\bar{\eta}_{shore}$ (not shown; see also Appendix C).

In addition to lowering the mean water level, the stems lower wave runup by nearly 32 cm, or 39%, at the shoreline (Figure 3a, Storm B). The reduction in runup and breaking wave height by seagrasses yields 2.2 m of avoided dune erosion (4.2 m of erosion in their absence compared to 2.0 m in their presence, Figure 3a). This estimate of avoided erosion does not take into account the fact that the depth-averaged undertow, the main mechanism for offshore sediment transport during storms, is weakened by the presence of vegetation. Indeed, as shown in Figure 2c, since wave height and, by extension, the mass flux of the waves are reduced [Equation (10)], the strength of the depth-averaged undertow U_{Off} decreases by more than 25% over the vegetated bed. Hence, it is likely that vegetation also reduces offshore sediment flux during storms and that mobilized sediments re-settle near the shoreline. The combination of those factors may facilitate a more efficient post-storm recovery.

We estimate the services of submerged vegetation under two additional simulated storm conditions (Table 2, Figure 3a). For storm A, vegetation reduces $\bar{\eta}_{shore}$ and total water level by

17 and 15 cm, respectively. For storm B, $\overline{\eta}_{shore}$ and total water level are reduced by 50 and 47 cm, respectively. Finally, through a combination of lower runup on the beach and reduced wave heights, the amount of shoreline erosion is reduced by roughly 50% (60 cm for storm A, and 5 m for storm C).

3.1.2   Role of Mean Current Advection and Bed Shear Stresses on the Mean Water Level

In the derivation of Equation (5) [*Dalrymple et al.*, 1984], the influence of mean currents is ignored. Accordingly, this term was neglected in the expression of $\overline{\eta}$, and Equation (16) simplified to Equation (17). In this section, we examine the role of mean current advection, and bed shear stresses to a lesser extent, in the computation of $\overline{\eta}$, using Equation (16).

In the absence of a reliable model for the expression of the undertow in the presence of vegetation, the undertow is assumed to be, as a first approximation, depth uniform in the vegetated field [i.e., $U_{Veg}(x,z) \cong U_{Veg}(x)$], and approximately an order of magnitude weaker than the orbital velocity, i.e., $\left| U_{Veg} \right| \cong u_{ow}/10$. These assumptions are reasonable based on experimental and numerical observations [*Lovas and Torum*, 2001; *Svendsen*, 2006; *Guannel*, 2009; *Maza et al.*, 2013]. At the bed, U_b is approximated by U_{Off} [*Guannel*, 2009].

The direction of the mean velocity in the presence of vegetation is still an active subject of research. Mean velocities in meadows have been observed to be directed both shoreward and offshore [*Lovas and Torum*, 2001; *Luhar et al.*, 2010, 2013]. This uncertainty is taken into account by considering both an offshore and a shoreward oriented mean velocity in the water column and at the bed. Thus, the effect of the formulation of mean stress on the water column is modeled using 4 combinations of velocity direction in the water column and at the bed.

For all combinations of stress formulation considered, vegetation lowers the mean water level at the shoreline, $\overline{\eta}_{shore}$ (Figure 3b). First, when vegetation-induced stresses are not taken into account ($\widetilde{F}_d = 0$), $\overline{\eta}_{shore}$ decreases by 11 cm on average (Figure 3b, Figure 2b). This reduction is solely due to the influence of vegetation on wave energy flux and radiation stress gradients (Figure 4a and b). When mean currents in the water column are oriented offshore ($U_{Veg} < 0$), the setup is reduced by 21 cm, on average. Changing the orientation of the bed shear stress ($U_b > 0$ or $U_b < 0$) only yields differences on the order of 6 cm. Finally, when the mean current in the meadow is oriented shoreward, $\overline{\eta}_{shore}$ is further lowered, resulting in an average reduction of 44 cm.

We also evaluated the influence of mean current and bed shear stresses on runup and erosion estimates (Figure 3b). In all cases, even when vegetation-induced stresses are ignored in the mean momentum equation, vegetation reduces total water level and shoreline retreat. On average, runup decreases by 12 cm when $\widetilde{F}_d = 0$, and by 38 cm when mean currents and bed shear stresses are included in the computation of $\overline{\eta}$. The impacts of a reduced mean water level on erosion estimates are more subtle, with erosion values varying by less than 1 m. This is likely due to the fact that the erosion model used herein is primarily controlled by wave breaking characteristics.

3.1.3   Balance of Stress Terms in the Mean Momentum Equation

To gain more insight into the potential role of the vegetation-induced stresses on $\overline{\eta}$, we examine the cross-shore structure of the various components of the mean momentum equation, for storm B. The balance of stress terms shows that, in the absence of vegetation, gradients in

radiation stress (∂S_{xx}, Figure 4a) oppose the pressure gradients caused by changes in $\bar{\eta}$ ($\partial \bar{\eta}$),

yielding a 49 cm setup at the shoreline. This balance is altered by the presence of vegetation.

The decrease in wave height in the shoaling region caused by vegetation (Figure 2a)

results in a decrease in radiation stress S_{xx}, which causes the gradient of S_{xx} to change sign

earlier along the profile ($x \cong 300$ m in Figure 4b compared to $x \cong 200$ m in Figure 4a). As wave

height decreases in the meadow, the radiation stress gradient becomes approximately 40%

weaker in the surf zone than when seagrasses are absent. This weakening of the radiation stress

gradient alone decreases wave setup to 37 cm, as observed in Figure 2b. The vegetation-induced

stress $\widetilde{F_d}$ reduces the setup further to 8 cm. In the shoaling and surf zone regions ($x < 200$ m,

Figure 4b), $\widetilde{F_d}$ is approximately twice as strong as the radiation stress gradient. This causes

gradients in $\bar{\eta}$ and S_{xx} to act together to oppose this stress, pushing shoreward the location of

the setdown, where the pressure gradient changes sign, and lowering the setup at the shoreline.

Finally, when offshore oriented mean currents are included in $\widetilde{F_d}$ (Figure 4c), they

generate a stress almost equal and opposite to the short-wave stress, cancelling the effect of $\widetilde{F_d}$

on the water column. As a consequence, the location of the maximum setdown moves further

offshore than when we only considered short-wave stresses, and the mean water level at the

shoreline increases to 32 cm. However, this setup is lower than when vegetation is absent

because the vegetation still modifies the profiles of the radiation stress gradient, as noted earlier.

The influence of bed shear stress is negligible in all cases.

3.2   Mangrove Forest on a Mud bed

The mangrove forest grows on a uniform 1V:600H mud bed. Seaward of the mangroves,

the seabed has a uniform slope of 1V:60H. The forest is composed of black mangroves

(*Avicennia germinans* species, see also Figure 1), and it extends landward from the shoreline for

250 m (Figure 5d). The physical characteristics of the aerial mangrove roots (pneumatophores)

and the trunks are, respectively: $h_{v1} = 0.5$ and $h_{v2} = 5$ m, $d_{v1} = 0.2$ and $d_{v2} = 30$ cm, and

$N_{v1} = 50$ and $N_{v2} = 0.7$ units/m^2 (Figure 1), where the subscripts 1 and 2 correspond to roots

and trunks, respectively. Following *FEMA* [2007], $C_{di,i=1,2} = 1$.

3.2.1   Quantification of Coastal Protection Services

The mangrove forest is subjected to the same storm conditions as the seagrass meadow

(Table 2). During storm B, waves break offshore of the mangroves (Figure 5a). In the surf zone,

wave height is reduced by an average of 73% across the forest, relative to the case without

vegetation (Figure 5a). The far field effect of the mangroves is more pronounced than in the

seagrass example, as waves exiting the forest remain lower than waves propagating over a non-

vegetated bed for more than 250 m. This pronounced far field effect is due to the fact that

mangroves are on a flatter bed than the seagrass and have a higher drag coefficient. Analysis of

profiles of wave energy dissipation (not shown) reveal that, because of the relatively shallow

water depth, the roots dissipate, on average, 80% more energy than the trunks.

In addition to attenuating waves, the mangrove forest also lowers $\bar{\eta}_{shore}$ by 13 cm, or

29%, compared to values obtained in the absence of vegetation (Figure 5b). Even if $\widetilde{F}_d$ is

neglected in the mean momentum equation, $\bar{\eta}_{shore}$ still decreases by 4 cm.

Finally, the attenuation of wave height due to the presence of vegetation nearly prevents

any sediment loss in the forest. When mangroves are present, the bed is only scoured over the

first 15 m (Figure 5c, $K_{veg} = 4$). By contrast, in the absence of mangroves, the bed is scoured

over its entire length. Even if the effect of the vegetation biomass is not taken into account (i.e.,

$K_{veg} = 1$), the reduced wave height and orbital velocity – due to the presence of the mangroves –
limit any scour to the first 60 m of the forest.

We conducted the same analysis for the two other hypothetical storms in Table 2 (Figure
6a). Overall, the mangrove forest reduces wave height by more than 65%, for all storms.
Vegetation also lowers $\bar{\eta}_{shore}$ by 7 cm for storm A, and 32 cm for storm C, and limits the loss of
sediment to the first few meters of forest, where scour rates decrease by more than 90%.
Therefore, mangroves, as modeled herein, appear to be particularly effective at reducing water
levels at the landward limit of flooded areas, as well as limiting the amount of sediment loss
during storms, compared to what would be observed in the absence of vegetation.

3.2.2   Role of Mean Current Advection and Bed Shear Stresses on the Mean Water Level

To evaluate the relative importance of mangrove-induced stresses, and the potential role
of mean currents on the mean water level, we assume that U_{Veg} is depth uniform, and that
$U_b \cong U_{Off}$. However, since the trees are emerged, the shoreward mass flux of the waves has to be
exactly balanced by the undertow [Equation (10)]. Thus, we only consider the case when U_{Veg} is
oriented offshore: $U_{Veg} \cong -\left|U_{Off}\right|$. The bed shear stress can act in either direction.

The role of the mangrove forest-induced stresses on $\bar{\eta}_{shore}$, for the three storm cases
(Figure **6b**), differs from what we observed in the seagrass example. First, when vegetation is
present but vegetation-induced stresses are ignored ($\widetilde{F_d} = 0$), $\bar{\eta}_{shore}$ is reduced by 8 cm, on
average. However, the inclusion of offshore oriented mean currents and bed shear stresses
increases $\bar{\eta}_{shore}$ to the point that it is nearly equal to the no-vegetation case. When the mean
current is still oriented offshore, but the bed shear stress is oriented shoreward, $\bar{\eta}_{shore}$ decreases

again by 9 cm, on average. However, it has nearly the same value of $\overline{\eta}_{shore}$ obtained when we took $\widetilde{F_d} = 0$.

These results indicate that the vegetation-induced mean current stress is likely to play an important role when vegetation is shoreward of the breaking region and waves are relatively small. However, our findings also point to the greater role played by bed shear stress in this example, as compared to the seagrass example. This is likely due to the fact that the depth average mean current is greater in that vegetation field by 30% on average.

3.2.3   Balance of Stress Terms in the Mean Momentum Equation

We again examine the balance of terms in the mean momentum equation (Figure **4**), for storm B, to better understand the potential importance of mangrove-induced stresses on $\overline{\eta}$. In the absence of vegetation, gradients of S_{xx} and $\overline{\eta}$ oppose each other (Figure 4d), yielding a setup of 45 cm at the shoreline. The rapid reduction of wave height caused by mangroves in the surf zone yields an initial 18% increase in the strength of the radiation stress gradient (Figure 4d and e, $x \cong 0$ m). However, as waves become smaller, the radiation stress gradient decreases by half near the landward edge of the mangrove ($x \cong 50$ m). This reduction alone would yield a lower setup of 41 cm at the shoreline (Figure 5b). However, because we take into account the vegetation-induced stress, which is, at its maximum, almost 40% as strong as the radiation stress gradient, the pressure gradient rapidly reduces to zero, further decreasing the setup at the shoreline to 33 cm. In contrast from the seagrass example, where seagrasses altered the shoaling and breaking process, mangroves are in the surf zone and the mangrove-induced stress works together with the pressure gradient to counteract the stress generated by the radiation stress gradient (Figure 4d and e). Hence, the location of setdown remains the same (Figure 4e and Figure **5**b).

Lastly, when we include the role of the offshore oriented undertow [Equation (16)], the stress that it generates opposes the short wave stress (Figure 4f), resulting in a higher pressure gradient in the first few meters of forest (increase of approximately 30% at $x \cong 0$). However, since the radiation stress gradient decreases as waves exit the forest, the pressure gradient also decreases. As a result, the setup at the shoreline increases to 40 cm. The bed shear stress plays a minor role.

Results presented in Sections 3.1 and 3.2 show that vegetation has the potential to modify mean water levels by altering the strength of radiation stress gradients, but also by generating relatively strong stresses in the water column. The direction and strength of the mean currents has the potential to either reinforce or reduce the importance of this stress. We confirmed this finding (not shown) by re-running the two cases presented above for storms A and C, assuming that vegetation could be represented using emergent stems [i.e., $\widetilde{F_d}$ is not approximated with Equation (13)], or by estimating U_{Veg} and U_b as 1/20 and 1/5 of the value of the orbital velocity respectively, and by estimating U_b with the formulation proposed by *Luhar et al.* [2010].

In summary, the application of our integrated modeling framework to two idealized examples demonstrates that vegetation has the potential to reduce the impacts of storms and thus provide important coastal protection services to people. These results also show that reliable models for the undertow in the presence of vegetation are imperative to better quantify the protective services provided by vegetation. Note that we only evaluated the potential role of the undertow in estimates of mean water level. The relative importance of this current in the dissipation of wave energy in the presence of vegetation [Equation (5)] was not quantified. In the next section, we examine the model's sensitivity to changes in vegetation characteristics, and suggest steps to improve the framework presented herein.

3.3   Relative Importance of Plant Parameterization and Choice of Drag Coefficient

The application of the proposed framework, or any model, to a particular site requires estimates of the physical characteristics of the vegetation at that site, along with an appropriate value of drag coefficient C_d. Plants' physical parameters are often challenging to measure [*de Vos*, 2004], and vary with regions, seasons, and ecosystem's health [*Feagin et al.*, 2011; *Paul and Amos*, 2011; *Pinsky et al.*, 2013]. Still, choosing an appropriate value of C_d is even trickier, as it requires wave measurements across the vegetation. Thus, it is common to use values of plant parameters found in the literature, which are measured under specific settings, forcing and plant conditions. In this section, the sensitivity of the model to plant parameters is investigated.

We assess the model's sensitivity to the choice of vegetation parameters using an uncertainty analysis method called tornado analysis [*Howard*, 1988; *Celona and McNamee*, 2001]. For simplicity, we use the seagrass meadow example (Section 3.1) – we obtained similar results for mangroves using values from *Narayan* [2009], or for marshes, using values from *Feagin et al.* [2011].

The first step in the tornado analysis is to define a range of possible values (minimum, typical, maximum) for N_v, h_v, d_v and C_d (Table 3). Values for N_v and h_v were obtained from *Huber* [2003], and for d_v by varying the diameter observed in *Huber* [2003] by a few millimeters, based on ranges observed elsewhere [*Pinsky et al.*, 2013]. Finally, a range of C_d values was generated from typical estimates obtained for seagrass meadows (see, e.g., *Pinsky et al.* [2013] or Appendix D). Next, the model is run multiple times for each value of a particular input variable (e.g., N_v), while keeping the other input variables (e.g., h_v, d_v and C_d) constant at their typical values. This step produces three model outputs for each particular variable. Differences between the output from the typical value and maximum and minimum outputs

values (the "swing") are plotted as horizontal bars. The longer the bar (or "swing") associated

with a particular variable, the more sensitive the model is to changes in that variable.

Results indicate that, in all cases, vegetation is likely to reduce the impact of storms

(Figure 7) since the swing is non-zero and lower than the output obtained from the typical

variable. However, variations in vegetation parameters can change the amount of protection

services supplied. More importantly, results clearly demonstrate that the choice of C_d dictates

most of the variance in modeled wave height, setup, and shoreline erosion. Changing the value of

C_d has the same effect on mean water level as the inclusion of mean current in the mean

momentum equation (Sections 3.1.2 and 3.2.2). Thus, the high uncertainty in the exact value of

drag coefficient yields results that mask the uncertainty in the theoretical framework.

This finding is somewhat troublesome, because it indicates the need for precise values of

C_d in the modeling framework. C_d values are difficult to obtain and measure, and are highly

variable in both time and space. Indeed, predictive formulas for C_d found in the literature are

highly dependent not only on the site where the study is conducted, but also on the wave model

used in the study (Appendix D). The sensitivity of the drag coefficient to setting and the choice

of wave model is partially due to the fact that many detailed processes are typically ignored in

Equation (5) (e.g., mean currents and other non-linear processes are neglected). In addition, little

is known about the specifics of how vegetation modifies wave breaking, which is typically

modeled based on tunable empirical formulations developed for beaches without vegetation

[*Mendez and Losada*, 2004; *Suzuki et al.*, 2012]. Finally, the model's sensitivity to C_d is also

due to the fact that the use of LWT yields an approximate estimate of the drag force generated by

vegetation – estimates of F_d using LWT differ by a factor of at least two from estimates made

using the more accurate stream function theory (Appendix A).

These results suggest that formulations of drag coefficient might only be reliable when used at the site where they were derived. If used at other sites, an uncertainty analysis might be required to capture the variability in protection metric estimates. However, some of the deficiencies of current estimates of C_d are currently being addressed by, e.g., decoupling C_d calibration from measurements using LWT [*Zeller et al,* 2014]. More observations of this type should help reduce model uncertainty.

4   Conclusion

This paper presents an integrated modeling framework for quantifying how vegetation can reduce the impacts of coastal hazards on coastal communities. Using two illustrative examples (a seagrass meadow offshore of a sandy beach backed by a dune and a mangrove forest on a mud bed), we first estimate changes in wave height during storms due to the presence of vegetation. We show that aquatic vegetation has the potential to lower mean water levels, using a newly derived formulation of the mean momentum equation. Then, relying on adapted formulations of runup and shoreline erosion models, we demonstrate that vegetation can reduce total water level, beach erosion and mud bed scour during storms.

By linking together some of the key wave-induced processes that lead to shoreline retreat, sediment loss and inundation, the framework allows for the quantification of coastal protection services supplied by coastal vegetation. Outputs from this model are in the units and of the type most relevant to practitioners, policymakers, and stakeholders. If necessary, they can be converted to monetary units as well (see InVEST documentation, *Sharp et al.* [2014]).

In addition to developing one of the first production functions to quantify the coastal protection services supplied by vegetation, this paper also highlights research needs that would allow for more accurate estimates of the protective role of vegetation. Specifically, there is a

need for a better understanding, and models, of the modification of wave breaking processes in the presence of vegetation. More importantly, additional field and laboratory observations of wave-induced velocity, mean water level, runup, beach erosion and mud bed scour in the presence of vegetation are critical to validate, improve or modify the integrated modeling framework proposed herein. Those observations are also necessary to better understand the role of mean currents on wave dissipation, mean water level and bed erosion in the presence of vegetation.

Lastly, this paper demonstrates that the variability of outputs from the model is most strongly dictated by the choice of drag coefficient. This can be interpreted positively since drag coefficient formulas, as currently computed and employed, are essentially calibration coefficients that capture processes that are ignored or approximated [*Mendez and Losada*, 2004; *Pinsky et al.*, 2013]. Thus, the filling of the theoretical gaps highlighted in this paper are likely to improve our ability to predict and choose a correct drag coefficient, which will allow for a more complete understanding and more accurate estimates of shoreline response in the presence of vegetation.

In conclusion, the integrated modeling framework presented in this paper is a critical first step toward the quantification of coastal protection services supplied by vegetation. It shows that vegetation can protect against storms, but that any quantification of that protection will contain significant uncertainty. This uncertainty will likely remain until there is a better understanding of the functional relationship between drag coefficients and wave parameters, as well as an understanding of the way in which vegetation modifies wave-induced nearshore processes. Thus, the framework, in its present form, is most appropriate for initial estimates of the effectiveness of nature-based solutions to coastal hazards and for developing initial alternative strategies for coastal disaster management.

References

Anderson, M. E., J. M. Smith, and S. K. Mckay (2011), *Wave Dissipation by Vegetation; Report ERDC/CHL CHETN I 82*, Vicksburg, MS.

Apotsos, A., B. Raubenheimer, S. Elgar, R. T. Guza, and J. A. Smith (2007), Effects of wave rollers and bottom stress on wave setup, *J. Geophys. Res.*, *112*(C2), C02003, doi:10.1029/2006JC003549.

Augustin, L. N., J. L. Irish, and P. Lynett (2009), Laboratory and numerical studies of wave damping by emergent and near-emergent wetland vegetation, *Coast. Eng.*, *56*(3), 332–340.

Baldock, T. E., and P. Holmes, S. Bunker, and P. Van Weert (1998), Cross-shore hydrodynamics within an unsaturated surf zone, *Coast. Eng.*, *34*, 173–196.

Battjes, J. A., and M. J. F. Stive (1985), Calibration and verification of a dissipation model for random breaking waves, *J. Geophys. Res.*, *90*(C5), 9159–9167.

Bradley, K., and C. Houser (2009), Relative velocity of seagrass blades: Implications for wave attenuation in low-energy environments, *J. Geophys. Res.*, *114*(F1), doi:10.1029/2007JF000951.

Bridges, A. (2008), The effect of model seagrass on wave runup: A laboratory investigation, 73 pp., University of Delaware.

Celona, J., and P. McNamee (2001), *Decision Analysis for the Professional*, 4th ed., edited by M. Campbel, B. Roehl, and M. Story, SmartOrg Inc.

Chen, S., L. Sanford, E. Koch, and F. Shi (2007), A nearshore model to investigate the effects of seagrass bed geometry on wave attenuation and suspended sediment transport, *Estuaries and Coasts*, *30*(2), 296–310.

Dalrymple, R. A., J. T. Kirby, and P. A. Hwang (1984), Wave Diffraction Due to Areas of Energy Dissipation, *J. Waterw. Port, Coast. Ocean Eng.*, *110*(1), 67–79.

Das, S., and J. R. Vincent (2009), Mangroves protected villages and reduced death toll during Indian super cyclone., *Proc. Natl. Acad. Sci. U. S. A.*, *106*(18), 7357–60.

Dean, R. G. (1965), Stream function representation of nonlinear ocean waves, *J. Geophys. Res.*, *70*(18), 4561–4572, doi:10.1029/JZ070i018p04561.

Dean, R. G. (1974), *Evaluation and Development of Water Wave Theories for Engineering Application; Special Report 1, Vols I and II*, Ft. Belvoir, VA.

Dean, R. G., and C. J. Bender (2006), Static wave setup with emphasis on damping effects by vegetation and bottom friction, *Coast. Eng.*, *53*, 149–156, doi:10.1016/j.coastaleng.2005.10.005.

Dean, R. G., and R. A. Dalrymple (1984), *Water wave mechanics for engineers and scientists*, Advanced Series on Ocean Engineering, edited by P. L.-F. Liu, World Scientific, Singapore.

Dean, R. G., and R. A. Dalrymple (2002), *Coastal processes with engineering applications*, Cambridge Univsersity Press, Cambridge, UK.

Feagin, R. A., S. M. Lozada-Bernard, T. M. Ravens, I. Möller, K. M. Yeager, and A. H. Baird (2009), Does vegetation prevent wave erosion of salt marsh edges?, *Proc. Natl. Acad. Sci. U. S. A.*, *106*(25), 10109–13.

Feagin, R. A., J. L. Irish, I. Möller, A. . Williams, R. J. Colón-rivera, and M. E. Mousavi (2011), Short communication: Engineering properties of wetland plants with application to wave attenuation, *Coast. Eng.*, *58*(3), 251–255.

Federal Emergency Management Agency (FEMA) (2007), *Guidelines for Coastal Flood Hazard Analysis and Mapping for the Pacific Coast of the United States*, Washington, D.C.

Guannel, G. (2009), Observations of Cross-Shore Sediment Transport and Formulation of the Undertow, Oregon State University.

Guannel, G., and H. T. Özkan-Haller (2014), Formulation of the undertow using linear wave theory, *Phys. Fluids*, *26*(5), 056604, doi:10.1063/1.4872160.

Le Hir, P., Y. Monbet, and F. Orvain (2007), Sediment erodability in sediment transport modelling: Can we account for biota effects?, *Cont. Shelf Res.*, *27*(8), 1116–1142.

Holthuijsen, L. H., and T. H. C. Herbers (1986), Statistics of Breaking Waves Observed as Whitecaps in the Open Sea, *J. Phys. Oceanogr.*, *16*(2), 290–297.

Howard, R. A. (1988), Decision Analysis: Practice and Promise, *Manage. Sci.*, *34*(6), 679–695.

Huber, C. (2003), Wave damping effects caused by seagrasses, 70 pp., Technical University of Hamburg.

Jadhav, R., and Q. Chen (2012), Field Investigation Of Wave Dissipation Over Salt Marsh Vegetation, in *33rd International Conference on Coastal Engineering*, edited by P. Lynett and J. M. Smith, Santander, Spain.

Jadhav, R. S., Q. Chen, and J. M. Smith (2013), Spectral distribution of wave energy dissipation by salt marsh vegetation, *Coast. Eng.*, *77*(null), 99–107.

Karambas, T., C. Koftis, E. Koutandos, and P. Prinos (2012), Innovative submerged structures/vegetation effects on coastal erosion: Numerical modeling of hydro-morphological processes, in *International Offshore and Polar Engineering Conference*, vol. 22, ISOPE, Rhodes, Greece.

Kobayashi, N., A. W. Raichle, and T. A. Asano (1993), Wave attenuation by vegetation, *J. Waterw. Port, Coast. Ocean*, *119*(1), 30–48.

Koftis, T., P. Prinos, and V. Stratigaki (2013), Wave damping over artificial Posidonia oceanica meadow: A large-scale experimental study, *Coast. Eng.*, *73*(null), 71–83, doi:10.1016/j.coastaleng.2012.10.007.

Kriebel, R. L., and R. G. Dean (1993), Convolution Method for Time-Dependent Beach-Profile Response, *J. Waterw. Port, Coast. Ocean Eng.*, *119*(2), 204–226.

Li, C. W., and M. L. Zhang (2010), 3D modelling of hydrodynamics and mixing in a vegetation field under waves, *Comput. Fluids*, *39*(4), 604–614.

Longuet-Higgins, M. S., and R. W. Stewart (1963), A note on wave set-up, *J. Mar. Res.*, *21*, 4–10.

Longuet-Higgins, M. S., and R. W. Stewart (1964), Radiation stresses in water waves; a physical discussion with applications, *Deep Sea Res.*, *11*(4), 529–562.

Lovas, S. M., and A. Torum (2001), Effect of the kelp Laminaria hyperborea upon sand dune erosion and water particle velocities, *Coast. Eng.*, *44*(1), 37–63, doi:10.1016/S0378-3839(01)00021-7.

Luhar, M., S. Coutu, E. Infantes, S. Fox, and H. Nepf (2010), Wave-induced velocities inside a model seagrass bed, *J. Geophys. Res.*, *115*(C12), C12005, doi:10.1029/2010JC006345.

Luhar, M., E. Infantes, A. Orfila, J. Terrados, and H. M. Nepf (2013), Field observations of wave-induced streaming through a submerged seagrass (Posidonia oceanica) meadow, *J. Geophys. Res. Ocean.*, *118*(4), 1955–1968, doi:10.1002/jgrc.20162.

Manca, E., I. Caceres, J. Alsina, V. Stratigaki, I. Townend, and C. L. Amos (2012), Wave energy and wave-induced flow reduction by full-scale model Posidonia oceanica seagrass, *Cont. Shelf Res.*, *null*(null), doi:10.1016/j.csr.2012.10.008.

Mariotti, G., and S. Fagherazzi (2010), A numerical model for the coupled long-term evolution of salt marshes and tidal flats, *J. Geophys. Res.*, *115*(F1), F01004, doi:10.1029/2009JF001326.

Maza, M., J. L. Lara, and I. J. Losada (2013), A coupled model of submerged vegetation under oscillatory flow using Navier–Stokes equations, *Coast. Eng.*, *80*(null), 16–34, doi:10.1016/j.coastaleng.2013.04.009.

Mazda, Y., M. Magi, and M. Kogo (1997), Mangroves as a coastal protection from waves in the Tong King delta, Vietnam, *Mangroves Salt marshes*, *1*(2), 127–135, doi:10.1023/A:1009928003700.

McIvor, A., T. Spencer, I. Möller, and M. Spalding (2012), *Reduction of Wind and Swell Waves by Mangroves; Natural Coastal Protection Series: Report 1; Working Paper 40*, Cambridge, UK.

McLachlan, A., and A. Dorvlo (2005), Global Patterns in Sandy Beach Macrobenthic Communities, *J. Coast. Res.*, *21*(4), 674–687.

Mendez, F. J., and I. J. Losada (2004), An empirical model to estimate the propagation of breaking and nonbreaking waves over vegetation fields, *Coast. Eng.*, *51*, 103–118, doi:10.1016/j.coastaleng.2003.11.003.

Méndez, F. J., I. J. Losada, and M. A. Losada (1999), Hydrodynamics induced by wind waves in a vegetation field, *J. Geophys. Res.*, *104*(C8), 18383, doi:10.1029/1999JC900119.

Möller, I., T. Spencer, J. R. French, D. J. Leggett, and M. Dixon (1999), Wave Transformation Over Salt Marshes: A Field and Numerical Modelling Study from North Norfolk, England, *Estuar. Coast. Shelf Sci.*, *49*(3), 411–426, doi:10.1006/ecss.1999.0509.

Mull, J. M., and P. Ruggiero (2014), Estimating exposure to storm-induced overtopping and erosion along U.S. West Coast dune backed beaches, *J. Coast. Res.*

Myrhaug, D., L. E. Holmedal, and H. Rue (2006), Erosion and deposition of mud beneath random waves, *Coast. Eng.*, *53*(9), 793–797, doi:http://dx.doi.org/10.1016/j.coastaleng.2006.03.004.

Narayan, S. (2009), The Effectiveness of Mangroves in Attenuating Cyclone- induced Waves, 114 pp., Delft University of Technology.

Nepf, H. M. (1999), Drag, turbulence, and diffusion in flow through emergent vegetation, *Water Resour. Res.*, *35*(2), 479–489, doi:10.1029/1998WR900069.

Nielsen, P. (1992), *Coastal Bottom Boundary Layers and Sediment Transport*, Advanced Series on Ocean Engineering, 1st ed., World Scientific.

Paul, M., and C. L. Amos (2011), Spatial and seasonal variation in wave attenuation over Zostera noltii, *J. Geophys. Res.*, *116*(C8), C08019, doi:10.1029/2010JC006797.

Pinsky, M. L., G. Guannel, and K. K. Arkema (2013), Quantifying wave attenuation to inform coastal habitat conservation, *Ecosphere*, *4*(8), art95, doi:10.1890/ES13-00080.1.

Raubenheimer, B., R. T. Guza, and S. Elgar (2001), Field observations of wave-driven setdown and setup, *J. Geophys. Res.*, *106*(C3), 4629–4638, doi:10.1029/2000JC000572.

Reniers, A. J. H. M., and J. A. Battjes (1997), A laboratory study of longshore currents over barred and non-barred beaches, *Coast. Eng.*, *30*, 1–22, doi:10.1016/S0378-3839(96)00033-6.

Ruessink, B. G., D. J. R. Walstra, and H. N. Southgate (2003), Calibration and verification of a parametric wave model on barred beaches, *Coast. Eng.*, *48*(3), 139–149.

Ruggiero, P., P. D. Komar, W. McDougal, J. Marra, and R. A. Beach (2001), Wave run-up, extreme water levels, and the erosion of properties backing beaches. Journal of Coastal Research, *J. Coast. Res.*, *17*(2).

Sharp, R. et al. (2014), *InVEST 3.0.0 User's Guide*, Stanford, CA.

Stockdon, H. F., R. A. Holman, P. A. Howd, A. H. Sallenger, and Jr. (2006), Empirical parameterization of setup, swash, and runup, *Coast. Eng.*, *53*(7), 573–588.

Suzuki, T., M. Zijlema, B. Burger, M. C. Meijer, and S. Narayan (2012), Wave dissipation by vegetation with layer schematization in SWAN, *Coast. Eng.*, *59*(1), 64–71, doi:10.1016/j.coastaleng.2011.07.006.

Svendsen, I. A. (2006), *Introduction to nearshore hydrodynamics*, Advanced Series on Ocean Engineering, edited by P. L.-F. Liu, World Scientific, Singapore.

Tallis, H. et al. (2012), A Global System for Monitoring Ecosystem Service Change, *Bioscience*, *62*(11), 977–986, doi:10.1525/bio.2012.62.11.7.

Thornton, E. B., and R. T. Guza (1983), Transformation of wave height distribution, *J. Geophys. Res.*, *88*(C10), 5925–5938.

U.S. Army Corps of Engineers (USACE) (2002), *Coastal Engineering Manual (CEM), Report EM 1110-2-1100*, Vicksburg, MS.

De Vos, W. J. (2004), Wave attenuation in mangrove wetlands; Red River Delta, Vietnam, 117 pp., T.U. Delft.

Wamsley, T. V, M. A. Cialone, J. M. Smith, J. H. Atkinson, and J. D. Rosati (2010), The potential of wetlands in reducing storm surge, *Ocean Eng.*, *37*(1), 59–68.

Whitehouse, R., R. Soulsby, W. Roberts, H. Mitchener, and HRWallingford (2001), *Dynamics of Estuarine Muds*, Thomas Telford Publishing, Heron Quay, London.

Wiegel, R. L. (1964), *Oceanographical engineering*, Prentice-Hall, Inc., Upper Saddle River, New Jersey.

Wu, W., M. Zhang, Y. Ozeren, and D. Wren (2013), Analysis of Vegetation Effect on Waves Using a Vertical 2D RANS Model, *J. Coast. Res.*, *287*, 383–397.

Zeller, R. B., J. S. Weitzman, M. E. Abbett, F. J. Zarama, O. B. Fringer, and J. R. Koseff (2014), Improved parameterization of seagrass blade dynamics and wave attenuation based on numerical and laboratory experiments, *J. Limnol. Oceanogr.*, *59*(1), 251–266, doi:10.4319/lo.2014.59.1.0251.

Zhang, K., H. Liu, Y. Li, H. Xu, J. Shen, J. Rhome, and T. J. Smith (2012), The role of mangroves in attenuating storm surges, *Estuar. Coast. Shelf Sci.*, *102-103*, doi:10.1016/j.ecss.2012.02.021.

Zhou, C. Y., and J. M. R. Graham (2000), A numerical study of cylinders in waves and currents, *J. Fluids Struct.*, *14*(3), 403–428.

Appendix A: Comparison of Drag Force Computed Using Linear Wave Theory and Stream Function Theory

To estimate the error associated with using LWT to compute F_d [Equation (1)], estimates of the non-dimensional wave-averaged drag force F_{nd} computed using LWT are compared to values obtained using stream function theory (SFT; *Dean* [1965]). F_{nd} is expressed as [*Dean*, 1974]:

$$F_{nd}(z_o) = \frac{2\overline{\int_{-h}^{-h+z_o} F_d \, \mathrm{d}z}}{\rho C_d b_v h H^2 / T^2} \qquad (A\text{-}1)$$

F_{nd} is computed with SFT following *Dean* [1974], and with LWT as $F_{nd}^{LWT}(z_o) = F_{nd}^{LWT}(h) z_o / h$, for $z_o < h$.

We computed F_{nd} at 10 discrete elevations ($z_o = 0.1h, 0.2h, \ldots, h$) through the water column, using various combinations of relative depths (h / L_o) and ratios of wave height over breaking wave height (H / H_b), assuming that $H_b = 0.78h$ (we used Cases 3, 4 and 5, A through D in the lookup tables of *Dean* [1974]). These combinations are reasonable representations of nearshore environments where vegetation exists.

The computed drag force using LWT varies almost linearly with the computed drag force using SFT ($R^2 > 0.8$, Figure A1), and the drag force computed from SFT also varies linearly with depth ($R^2 > 0.9$ [not shown]). Thus, the assumption of linearity between submerged and emerged stress in Equation (13) appears reasonable.

It also appears that estimates of the drag force using LWT can both over- and under-estimate the real drag force (Figure A1). For small relative depths ($h / L_o = 0.01$) and small waves (small ratios of H / H_b), LWT under-predicts the drag force compared to SFT (Figure A1). As the wave height increases toward its breaking height ($H / H_b \approx 1$), LWT over-predicts the force by more than factor of two. Further, as the relative depth increases, the over-prediction of the force by LWT increases. For $h / L_o = 0.05$, LWT overestimates the drag force by a factor of 2 to 4. When waves are in intermediate and deep water ($h / L_o > 0.05$), that factor is over 25 (Case 10, not shown).

Appendix B: Wave Dissipation and Mean Stress Terms due to the Presence of Vegetation

The dissipation terms due to the presence of vegetation in Equation (5) are expressed following *Suzuki et al.* [2012] as:

$$\begin{cases} D_{v1} = C_{d1} N_{v1} d_{v1} \left(\sinh^3 k\alpha_{v1}h + 3\sinh k\alpha_{v1}h \right) \\ D_{v2} = C_{d2} N_{v2} d_{v2} \left[\sinh^3 k(\alpha_{v1} + \alpha_{v2})h - \sinh^3 k\alpha_{v1}h + 3\sinh k(\alpha_{v1} + \alpha_{v2})h - 3\sinh k\alpha_{v1}h \right] \\ D_{v3} = C_{d3} N_{v3} d_{v3} \left[\sinh^3 k(\alpha_{v1} + \alpha_{v2} + \alpha_{v3})h - \sinh^3 k(\alpha_{v1} + \alpha_{v2})h + \ldots \right. \\ \left. \qquad 3\sinh k(\alpha_{v1} + \alpha_{v2} + \alpha_{v3})h - 3\sinh k(\alpha_{v1} + \alpha_{v2})h \right] \end{cases} \qquad \text{(B-1)}$$

where $\alpha_{vi} = \left[1 - \left(\sum_{k=1}^{i-1} h_{vk} \right) / h \right] - \left[1 - \left(\sum_{k=1}^{i} h_{vk} \right) / h \right] \mathcal{H}(h - h_{vi})$, with $\mathcal{H}$ the Heaviside step function.

For mangroves and trees, $i = 1$ corresponds to roots, $i = 2$ to trunks and $i = 3$ to canopies. For seagrasses and marshes, $i \equiv 1$ to represent stems and the subscript is omitted.

In the mean momentum equation, the mean current advection factors S_{vi} (Section 2.3.1)

are obtained by integrating $\cosh\left[k\left(h+z\right)\right]$ between the different layers that compose the

vegetation field:

$$
\begin{cases}
S_{v1} = \sinh k\alpha_{v1}h \\
S_{v2} = \sinh k\left(\alpha_{v1}+\alpha_{v2}\right)h - \sinh k\alpha_{v1}h \\
S_{v3} = \sinh k\left(\alpha_{v1}+\alpha_{v2}+\alpha_{v3}\right)h - \sinh k\left(\alpha_{v1}+\alpha_{v2}\right)h
\end{cases}
\tag{B-2}
$$

where expressions for the coefficients α_{vi} are presented above.

Appendix C: Runup

In order to test the assumption of linearity between estimates of $\bar{\eta}_{shore}$, the mean water level

at the shoreline computed from Equation (17), to $\bar{\eta}_{St}$, the empirical estimate of setup computed

from Equation (19), $\bar{\eta}_{shore}$ is compared with $\bar{\eta}_{St}$ for a wide range of equilibrium beach profiles, in

the absence of vegetation. The equilibrium beach profiles were generated from sediment sizes (

d_{50}) ranging from 0.1 to 1.09 mm [*Dean and Dalrymple*, 2002]. For each d_{50}, two types of

equilibrium profiles were created. The first type had a foreshore slope starting at 10 cm of water

depth, and the second had a foreshore slope that started at the intersection of the equilibrium

profile and a planar beach profile [*Kriebel and Dean*, 1993]. Foreshore slopes m varied from

1V:100H to 1V:10H and each d_{50} was related to four m values. Three m values were obtained

from *Wiegel* [1964], who proposed relationships for sheltered, moderately exposed and exposed

beaches. The fourth m value was obtained from *McLachlan and Dorvlo* [2005], who reported

observations of m as a function of d_{50} from beaches around the world. In total, 8 different profiles types were generated per d_{50}, for a total of 112 profiles.

To compute the maximum setup at the shoreline for a range of hydrodynamic conditions, we generated a distribution of wave heights between 0.5 and 12 m. For a given wave height value prescribed at the offshore boundary, a suite of associated wave periods was computed by letting offshore wave steepness range between $2x10^{-3}$ and 0.1 [*Holthuijsen and Herbers*, 1986], and limiting wave period to values lower than 20 s. This yielded a total of 402 combinations of wave height and period.

Results (Figure C1) indicate that, for a given foreshore slope value, there is a relatively strong linear relationship ($R^2 > 0.7$) between modeled maximum setup $\bar{\eta}_{shore}$ and $\bar{\eta}_{St}$.

Appendix D: Influence of Wave Model on Drag Coefficient Estimates

Here, we examine whether calibrated values of C_d are sensitive to the choice of wave model and formulations of the Reynolds number (R_e). The drag coefficient C_d is generally expressed as a function of R_e or Keulegan-Carpenter (KC) numbers (see *Anderson et al.* [2011] or *McIvor et al.* [2012] for a review). Table D1 lists several of the formulations of C_d as a function of R_e found in the literature; studies that did not use Equations (2) and (5) to compute C_d were neglected.

To test whether a general expression of C_d exists, we plotted together formulations of C_d versus R_e, regardless of the vegetation type (Figure D1). The scatter in the figure makes it clear that a strong universal relationship between these two dimensionless quantities is unlikely. Similar results were obtained when C_d was plotted as a function of KC , or when relationships were discriminated by taxa (results not shown). Consequently, many of the formulations for C_d

proposed in the literature are specific to the site and hydrodynamic conditions during which measurements were made. Next, we explore the sensitivity of C_d to the choice of wave model.

Pinsky et al. [2013] estimated the drag coefficient of a very large number of plants, under a wide range of hydrodynamic conditions, by fitting Equations (2) through (5) to observations. They also used the wave breaking model of *Baldock et al.* [1998] in Equation (2). However, formulations of C_d presented in the literature were obtained using other expressions of breaking dissipation as well as various definitions of the velocity u used to compute R_e. Indeed, u was defined as either the velocity at the beginning or at the middle of the vegetated field, and was computed either at the top of the submerged stems or near the bed [*Kobayashi et al.*, 1993; *Mendez and Losada*, 2004; *Le Hir et al.*, 2007; *Paul and Amos*, 2011; *Manca et al.*, 2012; *Jadhav et al.*, 2013; *Maza et al.*, 2013; *Wu et al.*, 2013].

To explore the sensitivity of the drag coefficient to the choice of a particular wave model and method to compute R_e, we re-analyzed the data in *Pinsky et al.* [2013]. In addition to the model of *Baldock et al.* [1998], we used the popular breaking dissipation models proposed by *Ruessink et al.* [2003], *Battjes and Stive* [1985], and by *Thornton and Guza* [1983] with breaking index values of $\gamma = 0.78$ and $\gamma = 0.42$. For each model, we set the breaking coefficient b equal to 0.6, 0.8 and 1.4, typical limits found in the literature. Finally, for each value of C_d obtained by fitting observations to the wave model, we computed four values of R_e by evaluating u at the different locations described above.

Results are presented in Figure D1, where the grey area represents the range and envelope of the C_d and R_e values computed. They indicate that the choice of breaking dissipation model, as

well as the way in which R_e is computed, significantly influence the value of the drag

coefficient.

Tables

Table 1: Table of frequently used notations, in alphabetical order

Symbol	Definition	Unit
α_{vi}	Ratio of the height h_{vi} of vegetation element i over the water depth h	-
η	Free surface elevation	m
$\bar{\eta}$	Mean water level (e.g., wave setup or setdown)	m
$\bar{\eta}_{shore}$	Mean water level at the shoreline computed from the mean momentum equation, Equation (17)	m
$\bar{\eta}_{St}$	Mean water level at the shoreline as computed in [*Stockdon et al.*, 2006], see Equation (20)	m
σ	Wave radial frequency	s^{-1}
τ_b	Bed shear stress	N/m^2
ψ	Wave phase ($\psi = kx - \sigma t$)	-
d_{vi}	Frontal distance (diameter) of vegetation elements	m
h	Still water level	m
h_{vi}	Height of vegetation elements	m
i	Vegetation element: $i = 1 - 3$, represents roots, trunk and canopy, respectively; for seagrasses. For seagrasses, $i \equiv 1$ and that subscript is omitted.	-
k	Wavenumber	m^{-1}
m	Beach foreshore slope	-
u	Horizontal velocity of water particles	m/s
u_b	Short-wave orbital velocity at the bed	m/s
u_{ow}	Magnitude of short-wave (orbital) velocity of water particles	m/s
x	Cross-shore position	m
z	Vertical position	m
B	Beach berm height	m
C	Wave celerity	m/s
C_{di}	Drag coefficient of vegetation elements	-
C_f	Friction coefficient	-
D	Beach dune height	m
D_b	Time averaged energy dissipation rate due to wave breaking	kW/m^2
D_f	Time averaged energy dissipation rate due to bottom friction	kW/m^2

D_v	Time averaged energy dissipation rate due to the presence of vegetation	kW/ m^2
E_r	Roller energy	J/m^2
E_w	Wave energy density	J/m^2
F_d	Drag force exerted by waves on vegetation stem or element	N/m^3
$\widetilde{F}_d$	Vegetation-induced stress in the water column	N/m^2
$\widetilde{F}_d^{Wave}$	Vegetation-induced stress in the water column generated by short-waves only	N/m^2
$\widetilde{F}_d^{U_{Veg}}$	Vegetation-induced stress in the water column generated by mean current in the vegetated field	N/m^2
H	Root-mean square wave height	m
H_o	Deep water significant wave height	m
N_{vi}	Density of vegetation field for vertical vegetation elements	units/m^2
R_u	Wave runup	m
R_e	Reynolds number	-
S_{xx}	Radiation stress generated by waves and rollers	J/m^2
T_p	Wave group peak period	s
U	Time average (mean) velocity of water particles	m/s
U_b	Near bed mean velocity	m/s
U_{Veg}	Mean velocity inside a vegetated field	m/s
U_{Off}	Depth averaged mean current (undertow) in the water column	m/s
W	Beach berm width	m

Table 2: Forcing conditions for the seagrass and mangrove case examples

Storm	Wave Height (m)	Wave Period (s)	Surge (m)
A	1.5	4.0	0.5
B	2.5	6.0	1
C	4	7	2

Table 3: Range of values for seagrass physical parameters

Variable	Minimum Value	Typical Value	Maximum Value
Density N_v (#/m^2)	240	1200	1500
Diameter d_v (mm)	0.4	6.0	7.5
Height h_v (cm)	20	40	60
Drag Coefficient C_d (-)	0.05	0.1	1.0

Table D1: List of studies that reported a drag coefficient as a function of Reynolds number

Study	Vegetation	Empirical Relation
Kobayashi et al. [1993]	Artificial kelp	$C_d = 0.08 + \left(\dfrac{2200}{R_e}\right)^{2.4}$ $2,000 < R_e < 18,000$
Méndez et al. [1999]	Artificial kelp - rigid	$C_d = 0.08 + \left(\dfrac{2200}{R_e}\right)^{2.2}$ $200 < R_e < 15,500$
Méndez et al. [1999]	Artificial kelp - swaying	$C_d = 0.40 + \left(\dfrac{4600}{R_e}\right)^{2.9}$ $2,300 < R_e < 20,000$
Bradley and Houser [2009]	Seagrass	$C_d = 0.1 + \left(\dfrac{925}{R_e}\right)^{3.16}$ $200 < R_e < 800$
Manca et al.	Seagrass	No Relationship; data points only

[2012]

Koftis et al.
[2013]

Seagrass

$$C_d = \left(\frac{2400}{R_e}\right)^{0.77}$$

$$R_e < 2500$$

Paul and Amos
[2011]

Marsh

$$C_d = 0.06 + \left(\frac{153}{R_e}\right)^{1.45}$$

$$100 < R_e < 1,000$$

Jadhav et al.
[2013]

Marsh

$$C_d = 0.02 + \left(\frac{4000}{R_e}\right)^{0.78}$$

$$200 < R_e < 3,500$$

Augustin et al.
[2009]

Cylinders

No relationship; data points only

Luhar et al.
[2013]

Seagrass

$$C_d = \left(\frac{837}{R_e}\right)^{1.6}$$

$$500 < R_e < 2500$$

Jadhav and Chen
[2012]

Marsh

$$C_d = 2\left(\frac{1300}{R_e} + 0.18\right)^{0.78}$$

$$600 < R_e < 3,200$$

USACE [2002]

Cylinders

$$C_d = 1.2 - 0.5\left(3.3\text{x}10^{-6} R_e - 0.667\right)$$

$$2\text{x}10^5 < R_e < 8\text{x}10^6$$
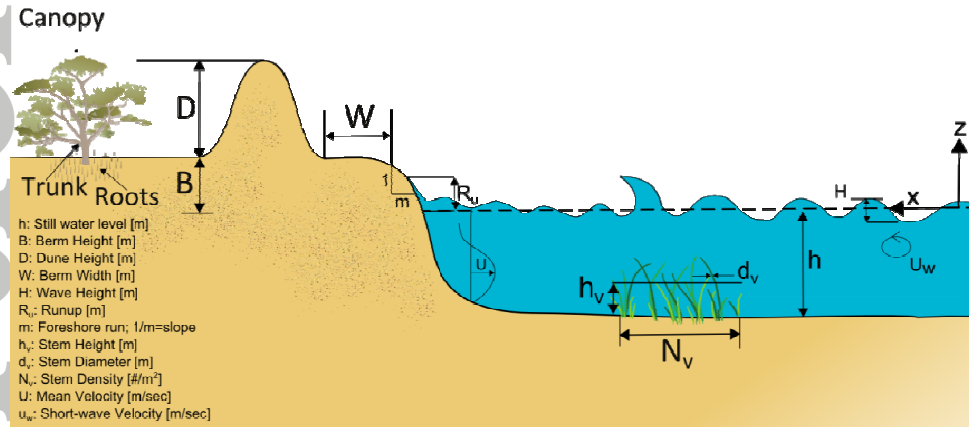
Figures

Figure 1: Definition sketch of main model variables.
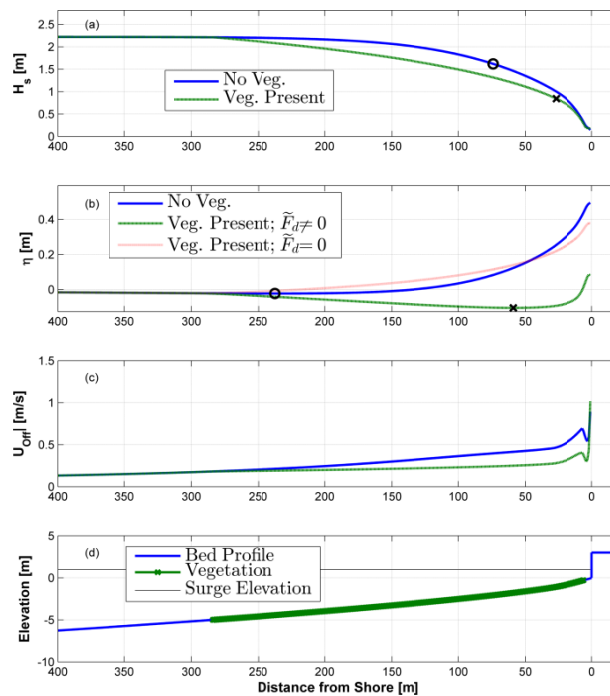
Figure 2: Wave model outputs for storm B (Table 2), for a seagrass bed offshore of a sandy

beach example. Top panel: profiles of wave height and location of wave breaking in the presence

and absence of vegetation (circle and cross, respectively). Second panel: profiles of mean water

level and location of minimum setdown (circle and cross), in the absence of vegetation, and in the presence of vegetation when vegetation-induced stress are taken into account ($\tilde{F}_d \neq 0$) and neglected ($\tilde{F}_d = 0$). Third panel: profiles of depth averaged undertow. Bottom panel: elevation profile showing the 3 m high dune and, the seagrass meadow location.
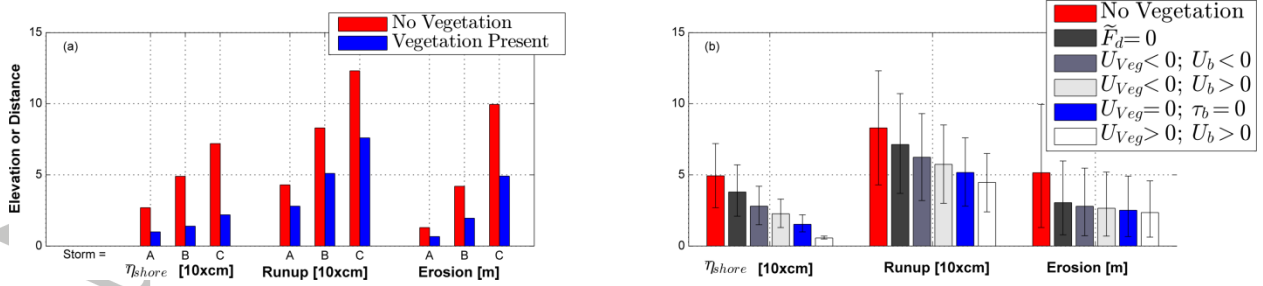
Figure 3: Model outputs, for storms A, B and C, for the seagrass example. Setup at the shoreline computed with Equation (17) is symbolized by $\overline{\eta}_{shore}$. Panel (a): outputs when vegetation-induced mean current stress ($\tilde{F}_d^{U_{Veg}}$) and bed shear stress (τ_b) terms are neglected in the mean momentum equation. Panel (b): outputs when $\tilde{F}_d^{U_{Veg}}$ and τ_b are included in the mean momentum equation. In that panel, the length of each vertical bar represents the mean value of the outputs variable for all three storm cases. Maximum and minimum values are shown as an error bar. Negative (positive) values of U_{Veg} and U_b indicate offshore (shoreward) oriented mean current and bed shear stresses, respectively.
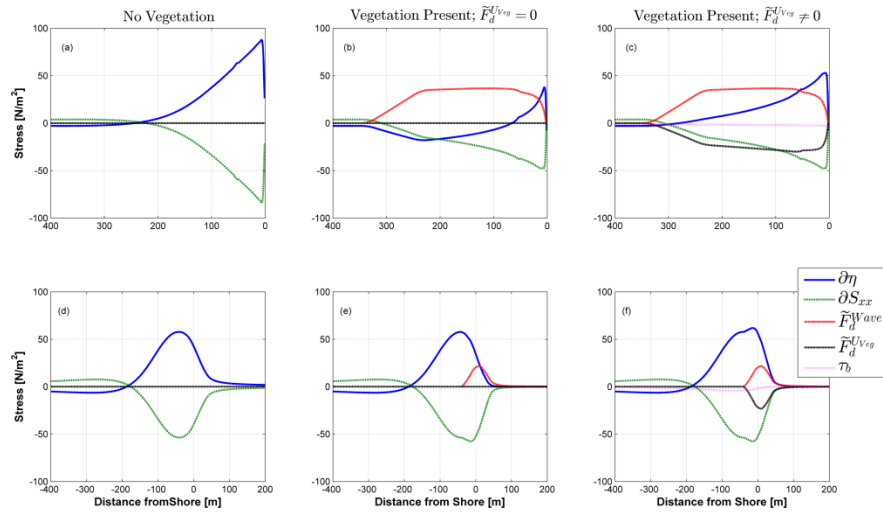
Figure 4: Balance of wave-induced stress terms, during storm B, for the seagrass (top panels) and mangrove forest (bottom panels) examples. Stress terms were computed in the absence of vegetation (left panels), in the presence of vegetation, but ignoring mean current and bed shear stresses (center), and by including those stress terms (right panels). In the legend, $\partial\eta$ refers to the pressure gradient term in Equation (16), ∂S_{xx} the radiation stress gradient, $\tilde{F}_d^{Wave}$ the short-wave stress, and $\tilde{F}_d^{U_{Veg}}$ the mean current stress term.
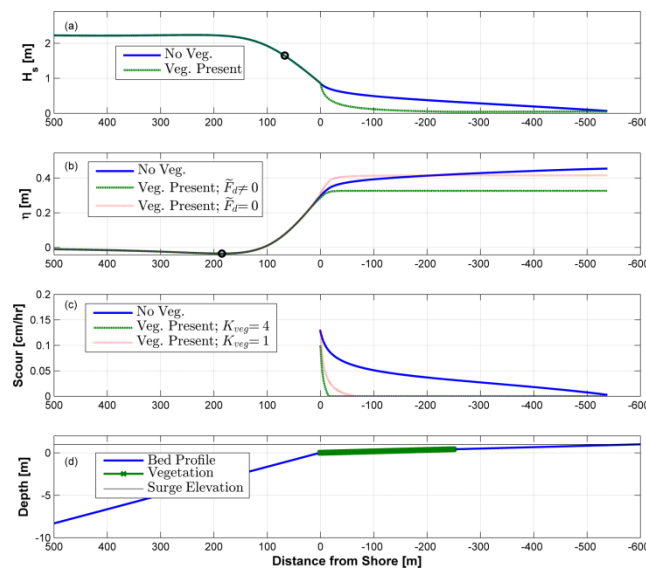
Figure 5: Wave model outputs for storm B (see Table 2), for the mangrove forest example. Top

panel: profiles of wave height and location of wave breaking (circle). Second panel: profiles of

mean water level and location of minimum setdown (circle), in the absence of vegetation, and in

the presence of vegetation when vegetation-induced stress are taken into account ($\tilde{F}_d \neq 0$) and

neglected ($\tilde{F}_d = 0$). Third panel: profiles of rate of mud bed scour. Effects of biota on critical bed

shear stress are taken into account when $K_{veg} = 4$, and neglected when $K_{veg} = 1$. Bottom panel:

depth profile showing the location of the mangroves.
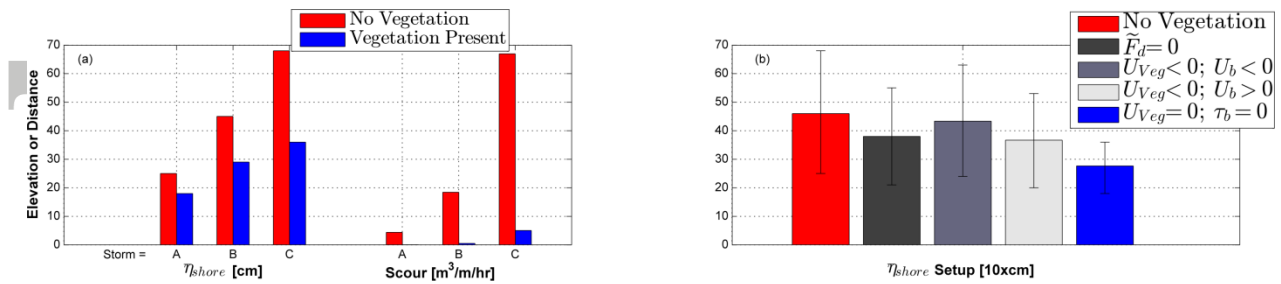
Figure 6: Model outputs, for storms A, B and C, for the mangrove forest example. Setup at the

shoreward end of the profile is symbolized by $\bar{\eta}_{shore}$. Panel (a): outputs when vegetation induced

mean current ($\tilde{F}_d^{U_{Veg}}$) and bed shear stress (τ_b) terms are neglected in the mean momentum

equation. Panel (b): Setup $\bar{\eta}_{shore}$ when $\tilde{F}_d^{U_{Veg}}$ and τ_b are included in the mean momentum

equation. In that panel, the length of each vertical bar represents the mean value of the setup for

all three storm cases. Maximum and minimum values are shown as an error bar. Negative

(positive) values of U_{Veg} and U_b indicate offshore (shoreward) oriented mean current and bed
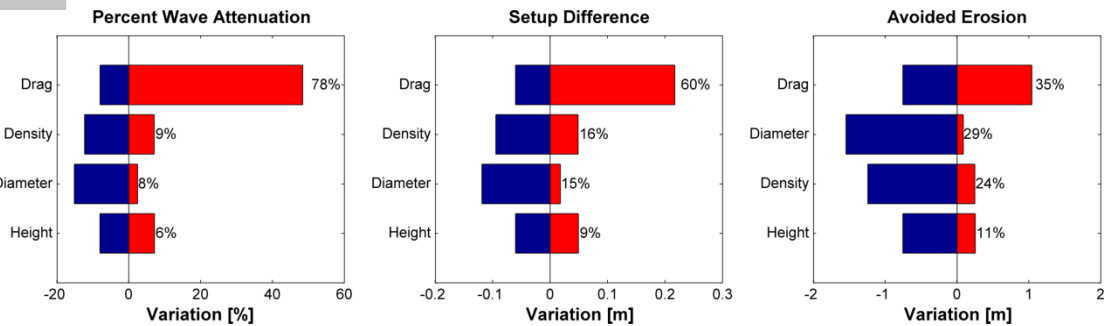
shear stresses, respectively.

Figure 7: Tornado diagram showing in the relative importance of vegetation height, diameter, density and drag coefficient on wave attenuation (left panel), setup difference (center) and avoided erosion (right). The percentage of the total variance of all outputs combined explained by a particular parameter is indicated next to each bar. For each parameter, the width of the red (blue) horizontal bar represents the difference between outputs obtained using typical values of all parameters – zero on the x-axis – and the output using the maximum (minimum) value of that parameter.
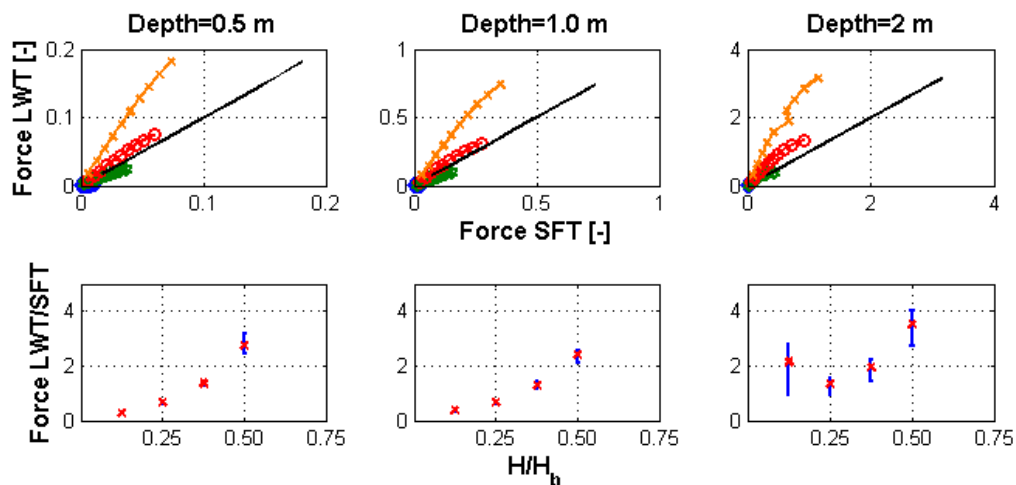
Figure A1: Comparison of non-dimensional drag force (F_d) computed using linear wave theory (LWT) and stream function theory (SFT) for different relative water depths. Top panels: F_d computed using LWT as a function of F_d computed using SFT for $H / H_b = 1$ (crosses), 0.75 (circles), 0.5 (hexagons), and 0.25 (diamonds). Bottom panels: ratios of non-dimensional drag force computed using LWT over the force computed using SFT, as a function of H / H_b. Vertical bars represent the maximum and minimum values of the ratio, crosses represent the average ratio.
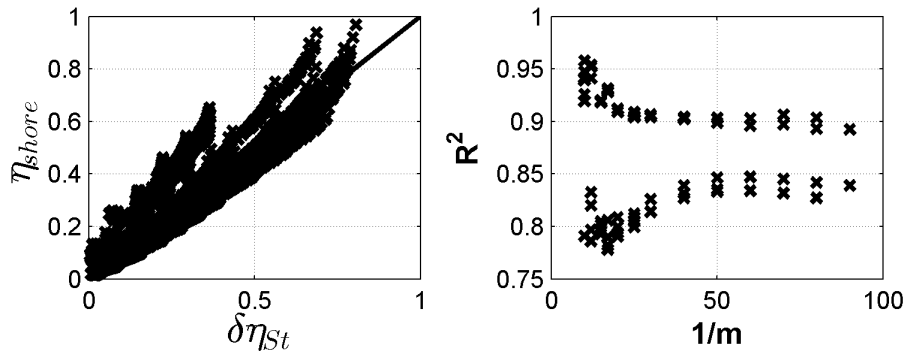

Figure C1: Relationship between setup computed using the formula of *Stockdon et al.* [2006] and the maximum setup computed using Equation (16), in the absence of vegetation. Left: maximum modeled setup $\bar{\eta}_{shore}$ as a function of setup from *Stockdon et al.* [2006] $\bar{\eta}_{St}$. The proportionality coefficient δ is unique for a given foreshore slope m. Right: R^2 value between $\bar{\eta}_{shore}$ and $\delta\bar{\eta}_{St}$ as a function of $1/m$.
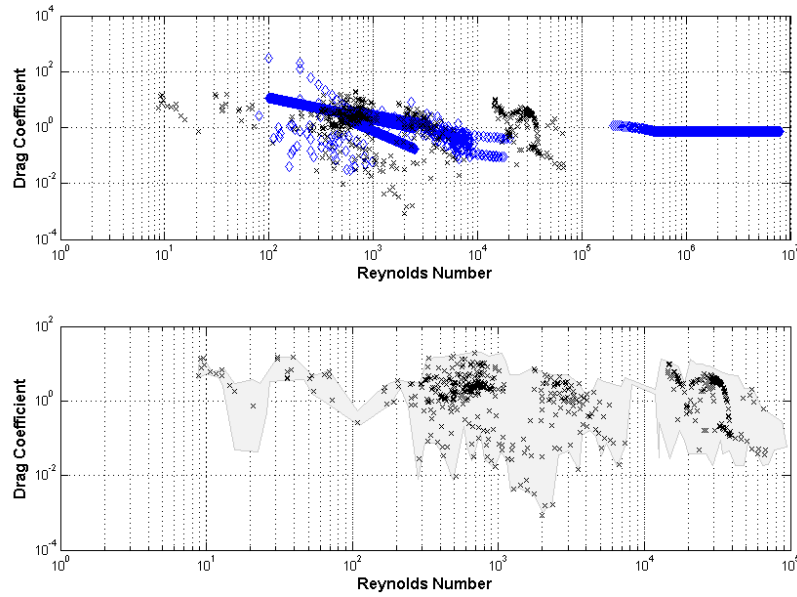
Figure D1: Relationship between drag coefficient C_d and Reynolds number R_e. Top: Values of C_d as a function of R_e published in various studies [diamonds, see Table D1] and computed by *Pinsky et al.* [2013] (crosses). Bottom: Values of C_d as a function of R_e computed by *Pinsky et al.* [2013] (crosses) superimposed on top of envelope of all values of C_d computed using the data in *Pinsky et al.* [2013] with different wave-breaking formulations.